Hollow-core photonic quasicrystal fiber with high birefringence and ultra-low nonlinearity

Zhuang Huo (霍 壮), Exian Liu (刘娥贤), and Jianjun Liu (刘建军)*

Key Laboratory for Micro/Nano Optoelectronic Devices of Ministry of Education & Hunan Provincial Key Laboratory of Low-Dimensional Structural Physics and Devices, School of Physics and Electronics, Hunan University, Changsha 410082, China

**Corresponding author: jianjun.liu@hnu.edu.cn*

Received October 25, 2019; accepted December 11, 2019; posted online March 10, 2020

A hollow-core fiber based on photonic quasicrystal arrays is theoretically proposed for high-quality light wave propagation with high polarization maintaining performance and low nonlinearity. This fiber, called hollow-core photonic quasicrystal fiber (HC-PQF), can simultaneously realize a high birefringence that reaches 1.345×10^{-2} and a small nonlinear coefficient of $1.63 \times 10^{-3}\ \mathrm{W}^{-1} \cdot \mathrm{km}^{-1}$ at a communication wavelength of 1.55 μm due to the air-filled core and unique quasiperiodic fiber structure. To further demonstrate the controllability of the nonlinear coefficient and the application of sensor and polarization-maintaining fiber, the nonlinearity is investigated by filling different inert gases in the fiber core while the birefringence keeps a high order of 10^{-2}. In the wavelength range $\lambda \in [1.53\ \mu\mathrm{m}, 1.57\ \mu\mathrm{m}]$, the dispersion is near zero and flattened. The HC-PQF is expected to be used for applications in optical communication, high power pulse transmission, polarization beam splitters, etc.

Keywords: fiber optics; fibers; polarization maintaining; photonic crystal fibers.
doi: 10.3788/COL202018.030603.

In the past three decades, photonic crystals have been widely used in couplers[1], lenses[2], all-optical logic gates[3], photonic crystal fibers (PCFs)[4–9], etc. The PCF has seen a rapid progress in multiple technical and scientific fields because of highly flexible arrangements of air-hole arrays and optimization of guiding characteristics. In addition to the periodic lattice in PCF the emerging quasiperiodic lattice structure that possesses a long-range orientational order and rotational symmetry has attracted tremendous interest for use in lenses[10], lasers[11], filters[12], sensors[13–15], topological photonics[16], etc. Among the applications, introducing a photonic quasicrystal structure in the fiber is a constructive means to highly enhance the basic guiding mode properties. It is reported that the constructed fiber, photonic quasicrystal fiber (PQF), can achieve near-zero dispersion[17], lower confinement loss[18], larger cut-off single mode transmission[19], higher mode area[20], robust transmission of orbital angular momentum mode[21], etc. Furthermore, PQF is also thought to show opposite negative dispersion behavior compared with PCF because of the unique fiber structure[22]. All research on PQFs employs solid-state cores (generally silica material) with a total reflection mechanism. However, the investigation on hollow-core PQF (HC-PQF) has not been reported although hollow-core PCF has been developed for many years for low transmission loss[18], low threshold of stimulated Raman scattering[23], etc. The difference between PQF and PCF is the difference between the quasiperiodic and periodic structures of the air-hole arrangement. The light guiding mechanism of the two fibers is consistent. Solid-core PCF is based on total reflection and HC-PCF is based on photonic band gap (PBG)[24]. Therefore, the light guiding mechanism of HC-PQF can be considered as that of HC-PCF based on the PBG effect. Benefitting from more geometrical degrees of freedom than HC-PCF, it has great potential in developing specific fiber with better optical properties and trade-off.

High birefringence enhances the polarization-maintaining ability to maintain the polarization state in the supercontinuum range. It has great application prospects in liquid crystal fiber[25] and polarization beam splitters[26], etc. The low nonlinear coefficient allows for high power pulse transmission[27], optical soliton transmission[28], pulse compression[29], etc. Combining high birefringence and low nonlinear coefficient characteristics, it has great potential for use in fiber sensors[30]. However, the birefringence of HC-PCF is relatively low, generally on the order of 10^{-3}[31–33], and most of the high birefringence PCFs proposed are accompanied by high nonlinear coefficients[34–36]. Therefore, how to improve the birefringence of HC-PCF and reduce its nonlinear coefficient are two subjects of great concern in the field of PCF. In 2018, Islam *et al.* proposed an HC-PCF[37] with a birefringence of 10^{-2}, but its core is filled with water, benzene, and ethanol, which makes its other optical properties unclear, and its preparation is difficult, so it is difficult to popularize and apply. In recent years, porous PCFs have been proposed to improve birefringence, and the birefringence reaches 10^{-2}[26,38], but the fiber core structure is complicated and difficult to prepare. Therefore, this Letter proposes the HC-PQF structure, which uses the quasiperiodic structure to destroy the symmetry to improve the birefringence. In addition, in order to make the fiber useable in special environments, this Letter tested the birefringence and nonlinear characteristics of two other inert gases.

In this Letter, an HC-PQF is proposed based on the six-fold photonic quasicrystal structure. At the communication wavelength of 1.55 μm, the birefringence reaches 1.345×10^{-2}. Compared to the solid-core PQF, when the core of the HC-PQF is filled with air, its nonlinear coefficient can be reduced by three orders of magnitude, and the nonlinear coefficient can be adjusted by the filling of a specific gas (e.g. argon or xenon). Therefore, the nonlinear coefficient can be controlled according to the different filling gases in the fiber core.

A six-fold photonic quasicrystal and the cross section structure of HC-PQF are shown in Fig. 1. The complete six-fold quasicrystal structure is shown in Fig. 1(a), which can be fabricated using a sol-gel method[39]. The lattice constant $\Lambda = 2.2$ μm, the diameter of the air hole is set to d, and the gray and white regions are silica and air with refractive indexes of $n_{\mathrm{SiO2}} = 1.45$ and $n_{\mathrm{air}} = 1.0$, respectively. The cross section structure of the HC-PQF designed in this Letter is shown in Fig. 1(b). The seven air holes in the blue dashed line circle in Fig. 1(a) are replaced by a hollow core with a diameter of d_1 as shown in Fig. 1(b). The nonlinear coefficient of HC-PQF can be adjusted by changing the material in the d_1 hole. Four red air holes in Fig. 1(a) are replaced by four small air holes with diameters $d_2 = 0.292 \times d$ and $d_3 = 0.62 \times d$ arranged symmetrically along the X axis in Fig. 1(b). The distance between the d_2 air hole and the d_1 hole is r, and the distance between the d_2 and d_3 air holes is $0.6 \times \Lambda$. Introducing small air holes in the center of the photonic quasicrystal structure and the X axis can destroy the symmetry of PQF and increase birefringence[40].

In this Letter, the COMSOL Multiphysics software[41] is used to simulate the proposed HC-PQF with perfect matching layer (PML) by the full vector finite element method, and the guiding characteristics of the HC-PQF under different wavelength and structural parameters are analyzed. The outermost blue ring is set to the PML, which allows the waves to pass through the interface without reflection, i.e., eliminating errors. The grid size is set to fine, which divides the whole HC-PQF into a large number of mesh elements that increase the analysis accuracy of fiber characterization, and the grid size is less than 5×10^{-8} m with an auto-triangular-mesh-subdivision method. After the program is started, under the premise of correctly setting the model, the calculated total number of mesh elements is 62,954 and the average element quality is 0.875. The structure mesh is of good quality, which is conducive to accurate calculations.

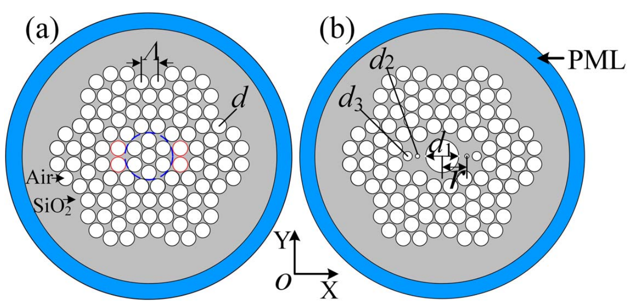

Fig. 1. (a) Cross section structure of the six-fold photonic quasicrystal (the origin O of the coordinate system OXY is set at the center of the fiber core); (b) the cross section structure of HC-PQF.

Birefringence is the difference of the effective refractive indexes of two orthogonal polarization modes. The higher the value is, the stronger the ability to maintain polarization is[42]. The equation is expressed as

$$B = \left| n_{\mathrm{eff}}^{y} - n_{\mathrm{eff}}^{x} \right|, \tag{1}$$

where n_{eff}^{x} and n_{eff}^{y} represent the effective refractive index of the fundamental mode in the x and y polarization directions, respectively.

In addition, the nonlinear coefficient of HC-PQF can be expressed as[43]

$$\gamma(\lambda) = \frac{2\pi n_2}{\lambda A_{\mathrm{eff}}}, \tag{2}$$

where n_2 is the nonlinear refractive index of the gas filled in the fiber core, and the effective mode field area A_{eff} can be calculated as[44]

$$A_{\mathrm{eff}} = \frac{\left(\iint \left| E^2 \right| \mathrm{d}x\mathrm{d}y \right)^2}{\iint \left| E \right|^4 \mathrm{d}x\mathrm{d}y}, \tag{3}$$

where the integral region is the entire cross section of fiber. According to Eq. (2), the larger the effective mode field area is, the smaller the nonlinear coefficient is.

The total dispersion $D(\lambda)$ can be deduced by the sum of the waveguide dispersion $D_w(\lambda)$ and the material dispersion $D_m(\lambda)$ as[44]

$$D(\lambda) = D_w(\lambda) + D_m(\lambda). \tag{4}$$

For HC-PQF, the material dispersion can be neglected when the fiber core is filled with gas. Therefore, the dispersion of HC-PQF is equal to the waveguide dispersion and can be expressed as

$$D(\lambda) = -\frac{\lambda}{c} \frac{\partial^2 \left| \mathrm{Re}(n_{\mathrm{eff}}) \right|}{\partial \lambda^2}. \tag{5}$$

The optimum solution of the fundamental mode field with a wavelength of $\lambda = 1.55$ μm is obtained by simulation calculation, as shown in Fig. 2.

Figures 2(a) and 2(b) show that the polarized E_x mode field of the fundamental mode is circular, and the polarized E_y mode field of the fundamental mode is elliptical and extends in the Y direction. This is due to the introduction of four smaller air holes in the X direction, which breaks the symmetry of the structure. Because the area of

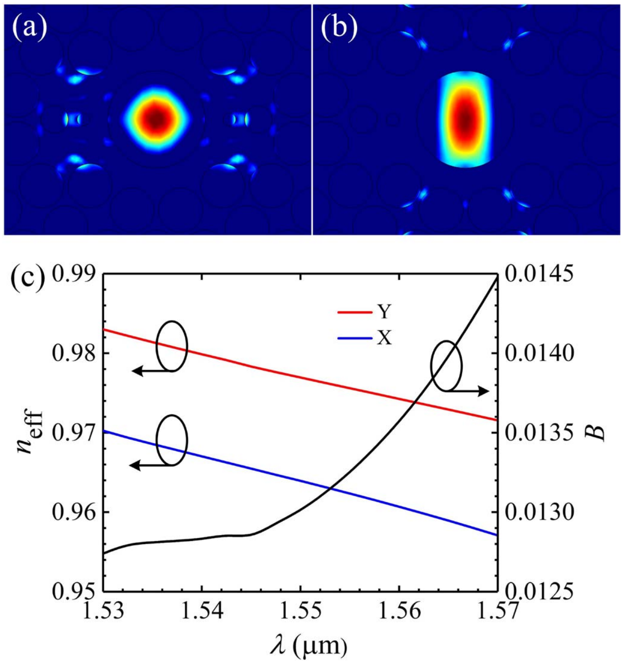

Fig. 2. Mode field distribution of HC-PQF: (a) direction of X polarization; (b) direction of Y polarization; (c) the effective refractive index of the X and Y polarization modes, and the corresponding birefringence.

four small air holes is smaller than that of four air holes with a diameter d, the filling ratio in the X direction is smaller than that in the Y direction. Because of the different structure of the fiber core region, the light propagates in different directions in the fiber core, making the effective refractive index in the X direction less than that in the Y direction, as shown in Fig. 2(c). Simulations for HC-PQF indicate that there are multiple modes of HC-PQF. Other modes are propagated through the cladding. When a specific wavelength of light passes through the waveguide, only the fundamental mode is excited for single mode transmission.

For a fixed $d/\Lambda = 0.910$, $r = 1.50\Lambda$, changing the hollow core diameter d_1 filled with air, the relationship between birefringence and wavelength is shown in Fig. 3.

Figure 3 shows that the birefringence increases with the increase of wavelength under a fixed d_1. When the wavelength $\lambda < 1.552$ μm and a certain wavelength are determined, as the hollow core diameter d_1 gradually increases, the birefringence gradually decreases. The main reason is that the increase of d_1 increases the core area, and the effect of the mode field and the inner cladding air holes is reduced, resulting in a decrease of birefringence. Therefore, in order to increase the birefringence, the structure with smaller diameters of air holes in the fiber core should be selected. When the wavelength $\lambda >$ 1.566 μm and a certain wavelength is determined, as the hollow core diameter d_1 gradually increases, the birefringence gradually increases.

Further calculations show that at the wavelength $\lambda = 1.55$ μm, the birefringence when the hollow core

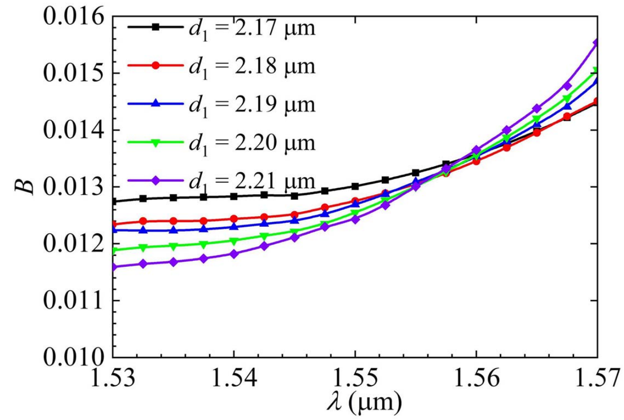

Fig. 3. Birefringence of HC-PQF under different d_1 values filled with air.

diameter $d_1 < 2.17$ μm is smaller than that when $d_1 = 2.17$ μm. When the wavelength $\lambda > 1.566$ μm and $d_1 < 2.17$ μm, the refraction disappears and the high birefringence characteristics are not satisfied. Therefore, $d_1 = 2.17$ μm should be selected in this structure. When $d_1 = 2.17$ μm and $\lambda = 1.55$ μm, the birefringence reaches 1.30×10^{-2}.

For a fixed hollow core diameter $d_1 = 2.17$ μm filled with air, $r = 1.50\Lambda$, changing the diameter of air hole d, the filling ratio d/Λ also changes. The relationship between birefringence and wavelength is shown in Fig. 4.

With the same filling ratio, as the wavelength gradually increases, as can be seen from Fig. 4, the birefringence gradually increases. With the increase of transmission wavelength, the mode field is increased. Therefore, it can be known that the mode field extends outward. But because the influence of the filling ratio in the X direction is smaller than that in the Y direction and light travels in air faster than in silicon, and since the inner air hole area is smaller than the ordinary air hole area, the distance of the mode field passing through the X direction is smaller than that of the mode field passing through the Y direction.

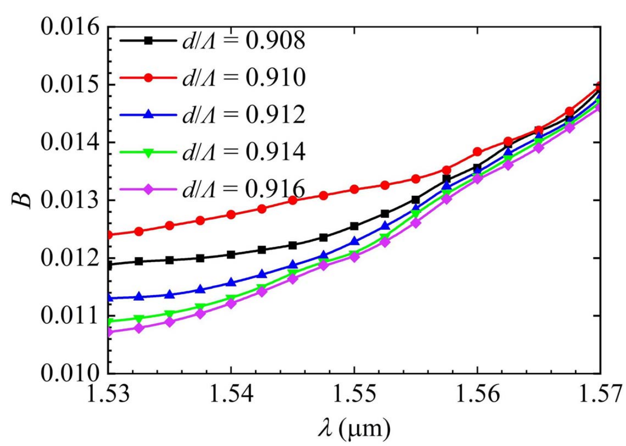

Fig. 4. When $d_1 = 2.17$ μm, the effect of filling ratio on birefringence.

Therefore, the mode field penetrates into the X direction and Y direction at different speeds. Thus, the birefringence increases gradually. At the same wavelength, as d/Λ increases, the birefringence first increases and then decreases, and reaches a maximum at $d/\Lambda = 0.910$. Therefore, the optimal value d/Λ in this structure is 0.910. When the wavelength $\lambda = 1.55$ μm, the birefringence reaches 1.32×10^{-2}. Its birefringence is two orders of magnitude higher than that in the traditional Panda polarization-maintaining fiber[45].

For a fixed ratio $d/\Lambda = 0.910$ and the hollow core diameter $d_1 = 2.17$ μm filled with air, the relative distance between the air holes of diameter d_3 and d_2 remains unchanged, and only the value of the distance r is changed. The relationship between birefringence and wavelength is shown in Fig. 5.

Figure 5 shows that the birefringence increases with the increase of wavelength at the same r. At the same wavelength, increasing r easily causes the mode field energy to penetrate from the fiber core, breaking the orthogonal polarization state and increasing the birefringence. In order to make the birefringence as large as possible, the maximum allowable value of r should be selected theoretically. However, when $r > 1.50\Lambda$, two small air holes of diameter d_3 overlap with air holes of diameter d, which is difficult to prepare, and the air holes collapse. Therefore, considering the size of birefringence and the difficulty of preparation, $r = 1.50\Lambda$ should be selected in this structure.

When $d/\Lambda = 0.910$, $d_1 = 2.17$ μm, $r = 1.50\Lambda$, at the wavelength $\lambda = 1.55$ μm, the birefringence reaches 1.345×10^{-2}. The structure design has a large degree of freedom, and many geometric parameters are related to birefringence, so the birefringence can be adjusted. In addition, a quasicrystal structure is adopted and small air holes are introduced around in the fiber core to break the periodicity to increase the birefringence. The birefringence is larger than that of HC-PCF at this stage[26,38].

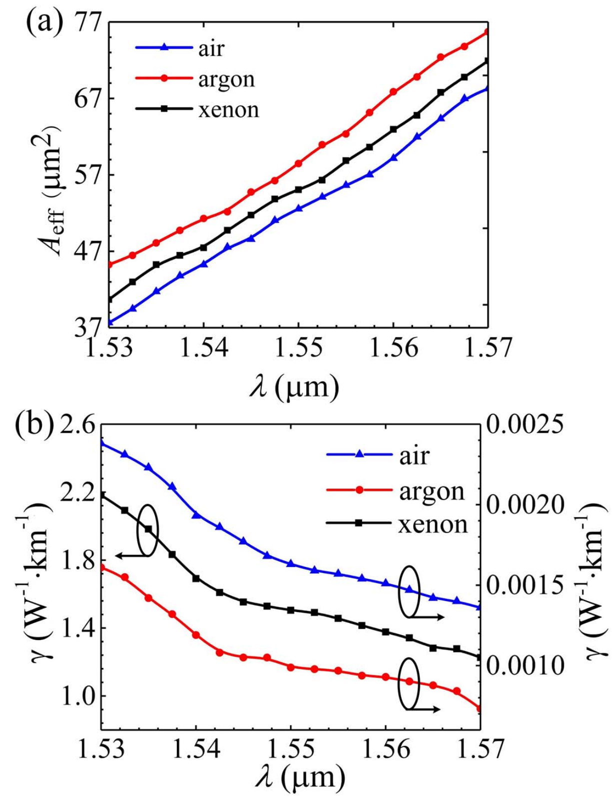

Fig. 6. $d/\Lambda = 0.910$, $d_1 = 2.17$ μm, $r = 1.50\Lambda$, changing the core filling gas: (a) the relationship between mode field area and wavelength, (b) the relationship between nonlinear coefficient and wavelength.

For a fixed $d/\Lambda = 0.910$, $d_1 = 2.17$ μm, and $r = 1.50\Lambda$, when the fiber core is filled with air, argon, and xenon, the relationship between mode field area and wavelength, and the relationship between nonlinear coefficient and wavelength, are shown in Figs. 6(a) and 6(b), respectively.

As can be seen from Fig. 6(b), the nonlinear coefficient decreases as the wavelength increases. On the one hand,

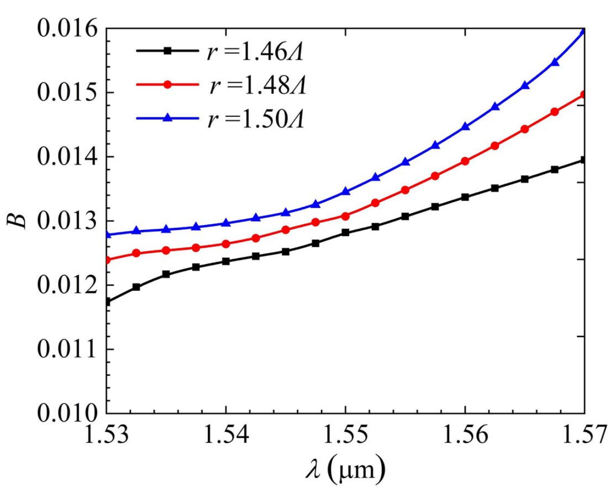

Fig. 5. When $d/\Lambda = 0.910$ and $d_1 = 2.17$ μm, the effect of changing the distance r between the d_2 small air hole and the fiber core on birefringence.

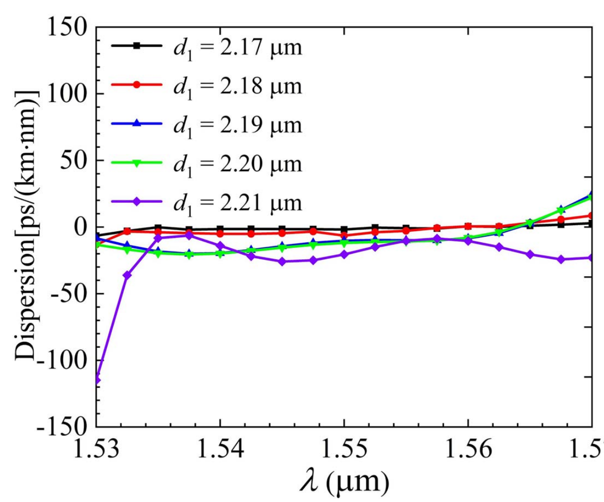

Fig. 7. Influence of the diameter of the hollow core on dispersion characteristics with $d/\Lambda = 0.91$ and $r = 1.50\Lambda$.

Table 1. Parameter Comparison of this HC-PQF with Previous Designs

PCF structure	Ref.	Birefringence	Nonlinear coefficient ($W^{-1} \cdot km^{-1}$)
PC-PCF	[34]	0.005	/
HC-PCF	[35]	5.8×10^{-3}	/
SGNLC-PCF	[36]	0.042	425.5
Proposed HC-PQF	This work	1.345×10^{-2}	1.63×10^{-3}

the wavelength increases; on the other hand, the effective mode field area of the structure proposed in this Letter increases with the increase of the wavelength. According to Eq. (2), the nonlinear coefficient decreases with increasing wavelength and effective mode field area.

When the fiber core is filled with air ($n_2 = 2.35 \times 10^{-23}\ \mathrm{m}^{-2} \cdot \mathrm{W}^{-1}$), the nonlinear coefficient is $1.63 \times 10^{-3}\ \mathrm{W}^{-1} \cdot \mathrm{km}^{-1}$ at the wavelength $\lambda = 1.55\ \mu\mathrm{m}$, which is ultra-low nonlinearity, and is generally three orders of magnitude smaller than that of solid-core fiber[44,46]. Under this circumstance, the structure satisfies the characteristics of high birefringence and low nonlinear coefficient. Under the premise of maintaining the birefringence of 10^{-2}, when the fiber core is filled with argon ($n_2 = 1.6 \times 10^{-23}\ \mathrm{m}^{-2} \cdot \mathrm{W}^{-1}$), the nonlinear coefficient is $1.0 \times 10^{-3}\ \mathrm{W}^{-1} \cdot \mathrm{km}^{-1}$. When xenon ($n_2 = 1.37 \times 10^{-20}\ \mathrm{m}^{-2} \cdot \mathrm{W}^{-1}$) is filled in the fiber core, the nonlinear coefficient is $1.50\ \mathrm{W}^{-1} \cdot \mathrm{km}^{-1}$ at wavelength $\lambda = 1.55\ \mu\mathrm{m}$, which is three orders of magnitude higher than that when the fiber core is filled with air. Therefore, the nonlinear coefficient in this fiber structure can be adjusted by changing the filler in the fiber core. The hollow core structure in this Letter provides a huge advantage when the gases, argon and xenon, are used to fill the fiber core to change the nonlinear coefficient. The filled gas has relatively stable chemical properties that will not change under some special circumstances, and it does not react with other substances. Therefore, the fiber structure in this Letter can be used in special environments.

As shown in Fig. 7, the smaller the diameter of the hollow core is, the more flattened the dispersion curve is. Considering the trade-off among birefringence, nonlinear coefficient, and dispersion, the value of the diameter of the hollow $d_1 = 2.17\ \mu\mathrm{m}$ can be chosen as the optimal value. At this time, the dispersion is relatively flattened and close to zero, $-1.05 \pm 1.28\ \mathrm{ps}/(\mathrm{km} \cdot \mathrm{nm})$, at the wavelength $\lambda \in [1.53\ \mu\mathrm{m}, 1.57\ \mu\mathrm{m}]$. Therefore, this structure can create conditions for achieving high-rate dense wavelength division multiplexing and frequency division multiplexing[47].

The performance parameter comparison between the proposed PCF and the previous works is shown in Table 1. It is clearly seen that the proposed HC-PQF can simultaneously exhibit polarization-maintaining ability and low nonlinearity, reaching a good level. Especially for the birefringence, the achieved value is more than twice higher than that of the previous HC-PCF[32,33].

In this Letter, an HC-PQF is proposed with high birefringence, and low and adjustable nonlinear coefficient properties. At the wavelength $\lambda = 1.55\ \mu\mathrm{m}$, the birefringence reaches 1.345×10^{-2}, and the ultra-low nonlinear coefficient when the fiber core filled with air is $1.63 \times 10^{-3}\ \mathrm{W}^{-1} \cdot \mathrm{km}^{-1}$. When the fiber core is filled with other gases (e.g., xenon or argon), the nonlinear coefficient can be adjusted while maintaining the birefringence of 10^{-2}. At the wavelength $\lambda \in [1.53\ \mu\mathrm{m}, 1.57\ \mu\mathrm{m}]$, the dispersion is flat dispersion. The structure has broad application prospects in the fields of sensors, polarization-maintaining fiber, high power pulse transmission, and long distance communication.

This work was supported by the National Natural Science Foundation of China (No. 61405058), the Natural Science Foundation of Hunan Province (No. 2017JJ2048), and the Fundamental Research Funds for the Central Universities (No. 531118040112). The authors acknowledge Prof. Jianqiang Liu for software sponsorship.

References

1. Z. Wang, K. Su, B. Feng, T. Zhang, W. Huang, W. Cai, W. Xiao, H. Liu, and J. Liu, Chin. Opt. Lett. **16**, 011301 (2018).
2. Y. Cen, J. Xie, and J. Liu, Chin. Opt. Lett. **17**, 080501 (2019).
3. C. H. Lu, B. Zhu, C. Y. Zhu, L. C. Ge, Y. Liu, Y. P. Chen, and X. F. Chen, Chin. Opt. Lett. **17**, 072301 (2019).
4. C. Liu, L. Yang, X. Lu, Q. Liu, F. Wang, J. Lv, T. Sun, H. Mu, and P. K. Chu, Opt. Express **25**, 14227 (2017).
5. J. Sultana, M. Islam, M. Islam, and D. Abbott, Electron. Lett. **54**, 61 (2018).
6. Z. K. Fan, IEEE Photonics J. **11**, 7101614 (2019).
7. C. M. Zhou, Y. D. Pang, L. Qian, X. Chen, Q. N. Xu, C. G. Zhao, H. R. Zhang, Z. W. Tu, J. B. Huang, H. C. Gu, and D. Fan, J. Lightwave Technol. **37**, 2568 (2019).
8. M. S. Islam, C. M. B. Cordeiro, J. Sultana, R. A. Aoni, S. L. Feng, R. Ahmed, M. Dorraki, A. Dinovitser, B. W. H. Ng, and D. Abbott, IEEE Access **7**, 79085 (2019).
9. M. Wang, F. Wang, and S. Y. Feng, Chin. Opt. Lett. **17**, 071401 (2019).
10. J. Liu and Z. Fan, IEEE Photonics Technol. Lett. **30**, 1001 (2018).
11. M. S. Vitiello, M. Nobile, A. Ronzani, A. Tredicucci, F. Castellano, V. Talora, L. H. Li, E. H. Linfield, and A. G. Davies, Nat. Commun. **5**, 5884 (2014).
12. Y.-F. Zhao, Z.-M. Wang, Z.-J. Jiang, X. Chen, C.-X. Yue, J.-Z. Wang, and J.-J. Liu, Int. J. Infrared Millimeter Waves **36**, 342 (2017).
13. C. Li, B. Yan, and J. Liu, J. Opt. Soc. Am. A **36**, 1663 (2019).

14. A. Shi, R. Ge, and J. Liu, Superlattices Microstruct. **133**, 106198 (2019).
15. Q. Liu, B. Yan, and J. Liu, Appl. Phys. Express **12**, 052014 (2019).
16. B. Yan, J. Xie, E. Liu, Y. Peng, R. Ge, J. Liu, and S. Wen, Phys. Rev. Appl. **12**, 044004 (2019).
17. R. Amezcua-Correa, N. G. R. Broderick, M. N. Petrovich, F. Poletti, and D. J. Richardson, Opt. Express **15**, 17577 (2007).
18. P. J. Roberts, F. Couny, H. Sabert, B. J. Mangan, D. P. Williams, L. Farr, M. W. Mason, A. Tomlinson, T. A. Birks, J. C. Knight, and P. S. J. Russell, Opt. Express **13**, 236 (2005).
19. E. Liu, B. Yan, W. Tan, J. Xie, R. Ge, and J. Liu, Superlattices Microstruct. **115**, 123 (2018).
20. E. Liu, W. Tan, B. Yan, J. Xie, R. Ge, and J. Liu, J. Opt. Soc. Am. A **35**, 431 (2018).
21. E. Liu, W. Tan, B. Yan, J. Xie, R. Ge, and J. Liu, J. Phys. D **52**, 325110 (2019).
22. B. K. Paul, M. A. Khalek, S. Chakma, and K. Ahmed, Ceram. Interfaces **44**, 18955 (2018).
23. F. Benabid, J. C. Knight, G. Antonopoulos, and P. S. J. Russell, Science **298**, 399 (2002).
24. K. Saitoh, N. J. Florous, T. Murao, and M. Koshiba, Opt. Express **14**, 7342 (2006).
25. D. C. Zografopoulos, E. E. Kriezis, and T. D. Tsiboukis, Opt. Express **14**, 914 (2006).
26. E. Reyes-Vera, J. Usuga-Restrepo, C. Jimenez-Durango, J. Montoya-Cardona, and N. Gomez-Cardona, IEEE Photonics J. **10**, 5900413 (2018).
27. J. D. Shephard, F. Couny, P. S. Russell, J. D. C. Jones, J. C. Knight, and D. P. Hand, Appl. Opt. **44**, 4582 (2005).
28. M. G. Welch, K. Cook, R. A. Correa, F. Gerome, W. I. Wadsworth, A. Y. Gorbach, D. Y. Skryabin, and I. C. Knight, J. Lightwave Technol. **27**, 1644 (2009).
29. A. A. Lanin, I. V. Fedotov, D. A. Sidorov-Biryukov, L. V. Doronina-Amitonova, O. I. Ivashkina, M. A. Zots, C. K. Sun, F. Omer Ilday, A. B. Fedotov, and K. V. Anokhin, Appl. Phys. Lett. **100**, 101104 (2012).
30. A. D. Kersey, M. A. Davis, H. J. Patrick, M. LeBlanc, K. P. Koo, C. G. Askins, M. A. Putnam, and E. J. Friebele, J. Lightwave Technol. **15**, 1442 (1997).
31. S. A. Mousavi, S. R. Sandoghchi, D. J. Richardson, and F. Poletti, Opt. Express **24**, 22943 (2016).
32. M. S. Islam, J. Sultana, K. Ahmed, M. R. Islam, A. Dinovitser, Ng. BWH, and D. Abbott, IEEE Sensors J. **18**, 575 (2018).
33. X. T. Zhao, Q. Xiong, G. H. Jiang, L. Hua, J. R. Cheng, and S. T. Wang, Opt. Fiber Technol. **46**, 167 (2018).
34. M. F. O. Hameed, S. S. A. Obayya, and H. A. El-Mikati, IEEE Photonics Technol. Lett. **23**, 1478 (2011).
35. Z. Q. Hui, Y. K. Zhang, and A. H. Soliman, Ceram. Interfaces **44**, 10383 (2018).
36. T. Y. Yang, C. Ding, and Y. J. Guo, IEEE Photonics J. **11**, 7200307 (2019).
37. M. S. Islam, J. Sultana, A. A. Rifat, A. Dinovitser, B. W. H. Ng, and D. Abbott, IEEE Sensors J. **18**, 4073 (2018).
38. J. Sultana, M. S. Islam, M. Faisal, M. R. Islam, B. W. H. Ng, H. E. Heidepriem, and D. Abbott, Opt. Commun. **407**, 92 (2018).
39. R. T. Bise and D. J. Trevor, in *2005 Optical Fiber Communications Conference* (2005), paper OWL6.
40. M. S. Islam, J. Sultana, A. Dinovitser, M. Faisal, M. R. Islam, B. W. H. Ng, and D. Abbott, Appl. Opt. **57**, 666 (2018).
41. COMSOL Multiphysics® Modeling Software: http://www.comsol.com/.
42. H. Wang, A. J. Yang, and Y. X. Leng, Laser Phys. **24**, 035101 (2014).
43. C. Jollivet, B. Samson, L. Leick, L. Shah, M. Richardson, and A. Schulzgen, Opt. Eng. **54**, 011006 (2015).
44. K. P. Hansen, Opt. Express **11**, 1503 (2003).
45. P. Romagnoli, C. R. Biazoli, M. A. R. Franco, C. M. B. Cordeiro, and C. J. S. de Matos, Opt. Express **22**, 17769 (2014).
46. K. Saitoh and M. Koshiba, Opt. Express **12**, 2027 (2004).
47. P. V. Mamyshev and L. F. Mollenauer, Opt. Lett. **24**, 448 (1999).